Charge-Driven Arrested Phase-Separation of Polyelectrolyte-Gold Nanoparticle Assemblies Leading to Plasmonic Oligomers

Florent Voisin, Gérald Lelong, Jean-Michel Guigner, Thomas Bizien, Jean-Maurice Mallet, Florent Carn

Journal Pre-proofs

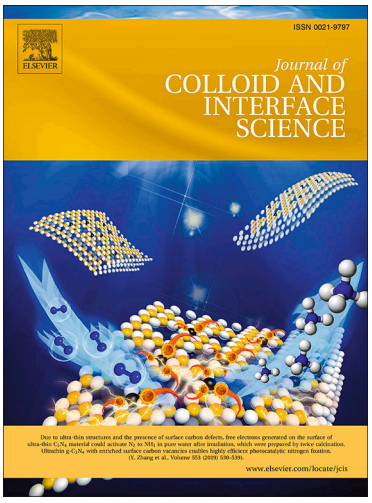

Charge-Driven Arrested Phase-Separation of Polyelectrolyte-Gold Nanoparticle Assemblies Leading to Plasmonic Oligomers

F. Voisin, G. Lelong, J.M. Guigner, T. Bizien, J.M. Mallet, F. Carn

PII: S0021-9797(22)01447-3
DOI: https://doi.org/10.1016/j.jcis.2022.08.076
Reference: YJCIS 30824

To appear in: *Journal of Colloid and Interface Science*

Received Date: 14 June 2022
Revised Date: 22 July 2022
Accepted Date: 11 August 2022

Please cite this article as: F. Voisin, G. Lelong, J.M. Guigner, T. Bizien, J.M. Mallet, F. Carn, Charge-Driven Arrested Phase-Separation of Polyelectrolyte-Gold Nanoparticle Assemblies Leading to Plasmonic Oligomers, *Journal of Colloid and Interface Science* (2022), doi: https://doi.org/10.1016/j.jcis.2022.08.076

Charge-Driven Arrested Phase-Separation of Polyelectrolyte-Gold Nanoparticle Assemblies Leading to Plasmonic Oligomers

F. Volsin,[1] G. Leloup,[1] J.M. Guigner,[2] T. Bizien,[3] J.M. Malet,[4] and F. Carn[1]*

[1] Laboratoire Matière et Systèmes Complexes, UMR 7057, Université de Paris, CNRS, Paris, France.
[2] Institut de Minéralogie, de Physique des Matériaux et Cosmochimie (IMPMC), Sorbonne Universités−UPMC Univ Paris 06, UMR CNRS 7590, Muséum National d'Histoire Naturelle, IRD UMR 206, F- 75005 Paris, France.
[3] Synchrotron Soleil, Beamline SWING, Gif SurYvette, Cedex F-91192, France
[4] Laboratoire des Biomolécules, UMR 7203, École Normale Supérieure, PSL Research University, Sorbonne Universités, CNRS, Paris, France.

* E-mail : florent.carn@u-paris.fr

Keywords. Gold, Chitosan, Nanoparticle, Polyelectrolyte, Self-Assembly, Complexation

Abstract

Aggregates of charged metal particles obtained by electrostatic coupling with a compound of opposite charge in the vicinity of the net zero charge ratio are of interest in the field of plasmonics because the inter-particle distance is minimal, which favours plasmonic coupling. However, these structures present a low colloidal stability limiting the development of applications. In this article we show that globally neutral aggregates formed by electrostatic complexation of citrate-stabilized gold particles and a quaternized chitosan (i.e., polycation) around the net zero charge ratio could be stabilized at a nanometric size by the subsequent addition of polyelectrolyte chains. Furthermore, the sign of the charge carried by the stabilizing chains determines the sign of the global charge carried by the stabilized complexes. The stabilization is demonstrated in saline environment on a broad pH range as well as in a cell culture media over periods of several days. Contrarily to stabilization by charged particles, our stabilized complexes are found to retain their initial characteristics (i.e. shape, size, internal structure and optical properties) after stabilization. Hence, the plasmonic coupling allows to maximize the optical absorption around the 800 nm wavelength at which the lasers used for thermoplasmonic and surface enhanced Raman scattering analysis operate.

1. Introduction

It has long been known that polyelectrolyte chains (PEL) could be added to a dispersion of oppositely charged colloids to promote colloid dispersion or to promote colloid

enough to saturate the colloid surfaces so as to keep them apart from each other.[4] In the second situation, long PEL having a contour length (L_c) much higher than the size of the colloids are usually added at a concentration close to the net zero charge ratio (ZCR) where the total charge of all PEL is compensated by the total charge of all colloids.[5–7] Here, the interest of using long chains close to the ZCR is to allow for the collection of several colloids per chain to speed up the formation of extended structures that sediment over time. At the local scale, PEL chains should wrap around the colloids but without necessarily covering the entire surface.[8,9] Thus, patches of opposite charge can coexist on the surface of the colloids in the vicinity of the ZCR even if the overall charge of the assembly is zero.[10]

Nevertheless, in certain conditions, long PEL chains can be used, both as coupling/adhesive agent and as a stabilising/repellent agent. Indeed, dispersions of finite size aggregates formed by the coupling of several colloids per PEL were obtained in the dilute domain of PEL concentration for low charge screening conditions and charge ratios far from the ZCR.[11–15] These so-called 'overcharged' aggregates or 'primary' complexes are nanometric and have a less dense structure than the complex coacervates (i.e. dense liquid phase) or precipitates (i.e. solid phase) obtained by working in the vicinity of the ZCR. This spatial distribution of the mass within the aggregate is generally characterized by the mass fractal dimension (d_f).[16] For particles with a mass, m_0, and a size, r_0, the total mass of the assembly, m, scales with its radius, r, measured from any site within the fractal structure, as $m(r) \propto m_0\left(r/r_0\right)^{d_f}$. $d_f \sim 2$ is typical of a random branched structure while $d_f \sim 1$ and $d_f \sim 2.9$ are expected for 1D and 3D structures respectively.[17] Interestingly, the average fractal dimension of overcharged aggregates could be modulated between 1 and 2.5 by playing on experimental levers such as the ratio between the effective PEL rigidity, quantified by the total persistence length ($L_{p,T}$), and the particle radius.[18,19]

Aggregates obtained in the vicinity of ZCR are characterised by a minimal inter-particle distance [10] and a high degree of compactness (i.e. $d_f \geq 2$) which can be associated with a high level of organisation with the possibility of forming colloidal crystals.[20] These structural specificities are in particular interesting for plasmonic applications because it could allow to

maximize the optical absorption around the 800 nm wavelength at which the lasers used for thermoplasmonic and surface enhanced Raman scattering analysis operate. [21,22]

However, such aggregates are effectively interesting if they can be stabilized soon after

has been poorly investigated so far with the exception of work carried out by the group of Stucky and Wong.[23] Their approach consisted first in forming globally neutral complexes of poly-L-Lysine (PLL) and citrate coated gold particles in the vicinity of the ZCR and then, to stabilize them by adding an excess of anionic silica particles. *In fine*, the stabilized complexes have a spherical vesicle structure with a water-filled core and a two-part shell. The inner part of the shell consists mainly of gold and PLL while the outer part is mainly composed of silica particles. The final vesicle structure is therefore different from the initial fractal structure. The mechanism of reorganization following the addition of the silica particles has not been clearly established. Following this seminal study, neutral complexes of different natures (i.e. polycation/polyanion,[24] multivalent ion/polyelectrolyte[25–27]) were stabilized by the subsequent addition of nanoparticles[24–26] or antibody molecules[27] always leading to the same type of vesicle structures. We also highlight the extensive work of Schneider and Decher showing how a wide range of different morphologies and compositions of "nanobags" can be obtained in aqueous suspension by the one-step mixing of polyelectrolytes, multivalent ions and nanoparticles in different ratios and concentrations.[28]

The objective of the present work is to stabilise electrostatic complexes of PELs and nanoparticles formed at the ZCR by the subsequent addition of PEL chains. To our knowledge, this possibility has never been reported so far. As a case study, we considered classical citrate coated gold nanoparticles of different sizes and linear PELs chains of natural origin which were quaternized chitosan (i.e. polycation, noted QC) and hyaluronic acid (i.e. polyanion, noted HA). We have systematically characterized the size, structure and optical properties of the PEL/particles assemblies by performing dynamic light scattering (DLS), small-angle X-ray scattering (SAXS), cryogenic transmission electronic microscopy (cryo-TEM) observations and UV-Vis.-NIR spectroscopy measurements. Our main result is that globally neutral aggregates could be stabilized at a nanometric size by the subsequent addition of PEL chains. This stabilisation is demonstrated in saline environment on a broad pH range as well as in a cell culture media over periods of several days. Contrarily to particle-stabilized complexes developed by Stucky and Wong, PEL-stabilized complexes are found to retain their initial characteristics (i.e. shape, size, internal structure and optical properties) after stabilization. Furthermore, the charge of the stabilizing chains determines the global charge of the stabilized

complexes which offers interesting possibilities of post-functionalization. We believe that the stabilization mechanism is based on the adsorption of stabilizing chains on oppositelly charged domains on the surface of the globally neutral aggregates.

Our core methodology consists of forming globally neutral complexes of QC chains (i.e. linear polycation) and citrate coated AuNP (i.e. spherical polyanion) and then injecting a QC solution to stop the growth of the aggregates as illustrated in scheme 1. These 2 stages will be called 'coupling' and 'quenching' stage respectively afterwards.

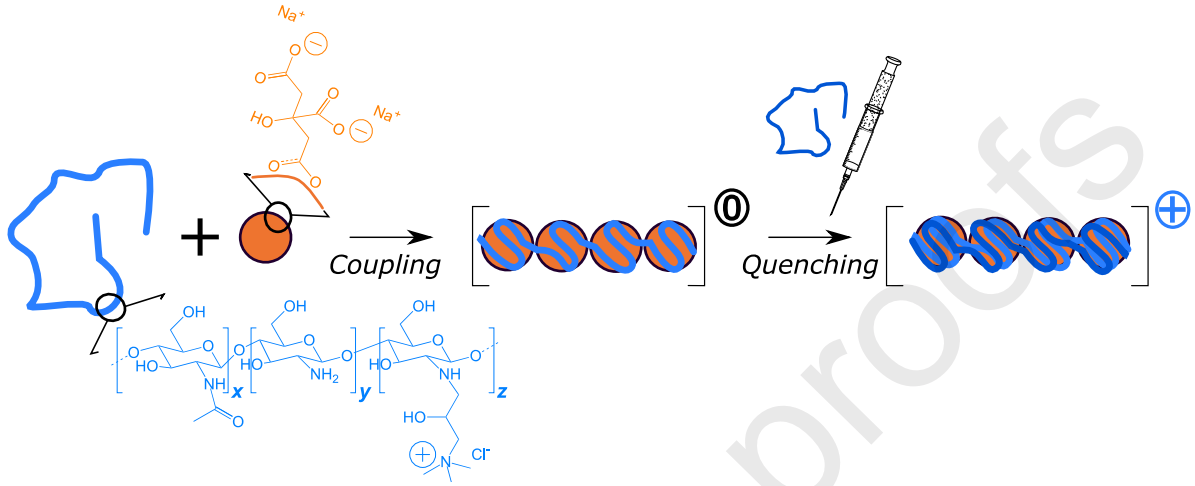

Scheme 1. Schematic illustration of the methodology used for the stabilisation of globally neutral aggregates composed of quaternized chitosan (QC) and citrate coated gold nanoparticles (AuNP).

2.1 Complexation between AuNPs and quaternized chitosan.

The coupling has been realized by equivolumic mixing of AuNP with radius R ≈ 11.5nm (Figure 1 of Supporting Information (SI)) and QC with Lc ≈ 1 µm (Figure 2 of SI) in milliQ water at pH ≈ 6.5. The AuNP concentration has been fixed at 1.3×10^{12} NP/mL while the QC concentration has been varied, staying in the diluted regime, to cover 4 decades of molar ratio, noted $\chi = n_{PEL} / n_{AuNP}$, with $0.035 \leq \chi \leq 35$.

QC-AuNPs assemblies were first studied by DLS (Figure 1a) and laser Doppler electrophoresis (Figure 1b). We detected finite size assemblies with negative or positive global charge 2 min after mixing at low and high molar ratio, respectively:

- for $\chi \leq 0.14$: $\mu \approx -2.8 \times 10^{-8}$ $m^2V^{-1}s^{-1}$ and $R_H = 34.7$ nm;
- for $\chi \geq 0.7$: $\mu \approx 1.2 \times 10^{-8}$ $m^2V^{-1}s^{-1}$ and $R_H = 34.7$ nm.

Contrary to previous results obtained at pH = 3 with non-quaternized chitosan chains,[29] these overcharged complexes show good colloidal stability for 24 h. The measured

net zero charge ratio corresponds to χ^*~ 0.28. As expected, the globally neutral assemblies obtained around χ^* grow rapidly to form micrometric structures that completely sedimented after few hours. We estimate that χ^* corresponds to a charge ratio, $\left({}^{n_+}/_{n_-}\right) \approx 0.2$,

using the structural charges (i.e. ~ 1736 e/chain and ~ 3324 e/NP with 2e/nm² [30]). The same calculation taking into account the effective charges including the effect of the condensed counterions (i.e. ~ 1438 e/chain and ~ 66 e/NP [31]) would be equal to $\left({}^{n_+}/_{n_-}\right)_{Effective} \approx 6.1$. It appears that the measured value of χ^* is in good agreement with the calculations within the uncertainties and considering that the measured χ^* may result from a partial compensation of the charges on a local scale whereas the measured electrophoretic mobility is zero.

The structure of the complexes was then studied by SAXS (Figure 1b). All the curves superimpose at $q \geq 0.06$ Å^{-1} showing that the structure and concentration of the scatterers is similar at this scale. Indeed, the particle concentration is constant while the contribution of QCs to scattering is much lower than that of AuNPs. This part of the curves is thus well described by the form factor of polydisperse spheres with R ≈ 11.5 nm in accordance with TEM images (Figure S1). The curves differ for $q < 0.06$ Å^{-1}. At low χ, the curves tend towards a plateau following the form factor of isolated spheres. This shows that the signal is probably dominated by AuNPs in excess, i.e. not involved in the assemblies. Around χ^*(i.e. for χ = 0.35 and 0.7), I(q) increases as a power law with an exponent ~ 2 corresponding to the average mass fractal dimension (d_f) expected for random branched structures. At low q, the curves do not reach the Guinier regime which indicates that the complexes are larger than 300 nm in agreement with DLS. In excess of QC (i.e. $\chi \geq 0.1$), d_f stabilizes at about 2 without detectable contribution from free QC chains in excess. Furthermore, it can be noted that the size of the objects decreases, keeping their structure, in excess of NP (χ = 0.025) and QC (χ = 6.2) with overlapping curves. Overall, the evolution of d_f with χ has a bell shape with a maximum around χ^* (Figure 1e).

This structural study was completed by observing QC-AuNPs assemblies obtained 2 min after mixing at selected χ by cryoTEM (Figures 1c and S3). Additional images are shown in the figure S3 of SI. At χ^*, all particles are involved in large aggregates with an average aggregation number, $N_{Agg} \approx 83$, and a branched structure compatible with $d_f \sim 2$. As expected for such out-of-equilibrium electrostatic assembly, the aggregate are polydisperse in size (Figures 1c, S3c). Interestingly, the assemblies obtained on both sides from χ^*, at χ = 0.14 and

χ = 0.7, are small (i.e. $N_{Ag.} \approx 4$) and coexist with individual AuNPs. The proportion of these non-aggregated particles among the aggregates is of the order of 10% and 17% for χ = 0.14 and χ = 0.7 respectively, whereas only 5% are counted for $\chi = \chi^*$.

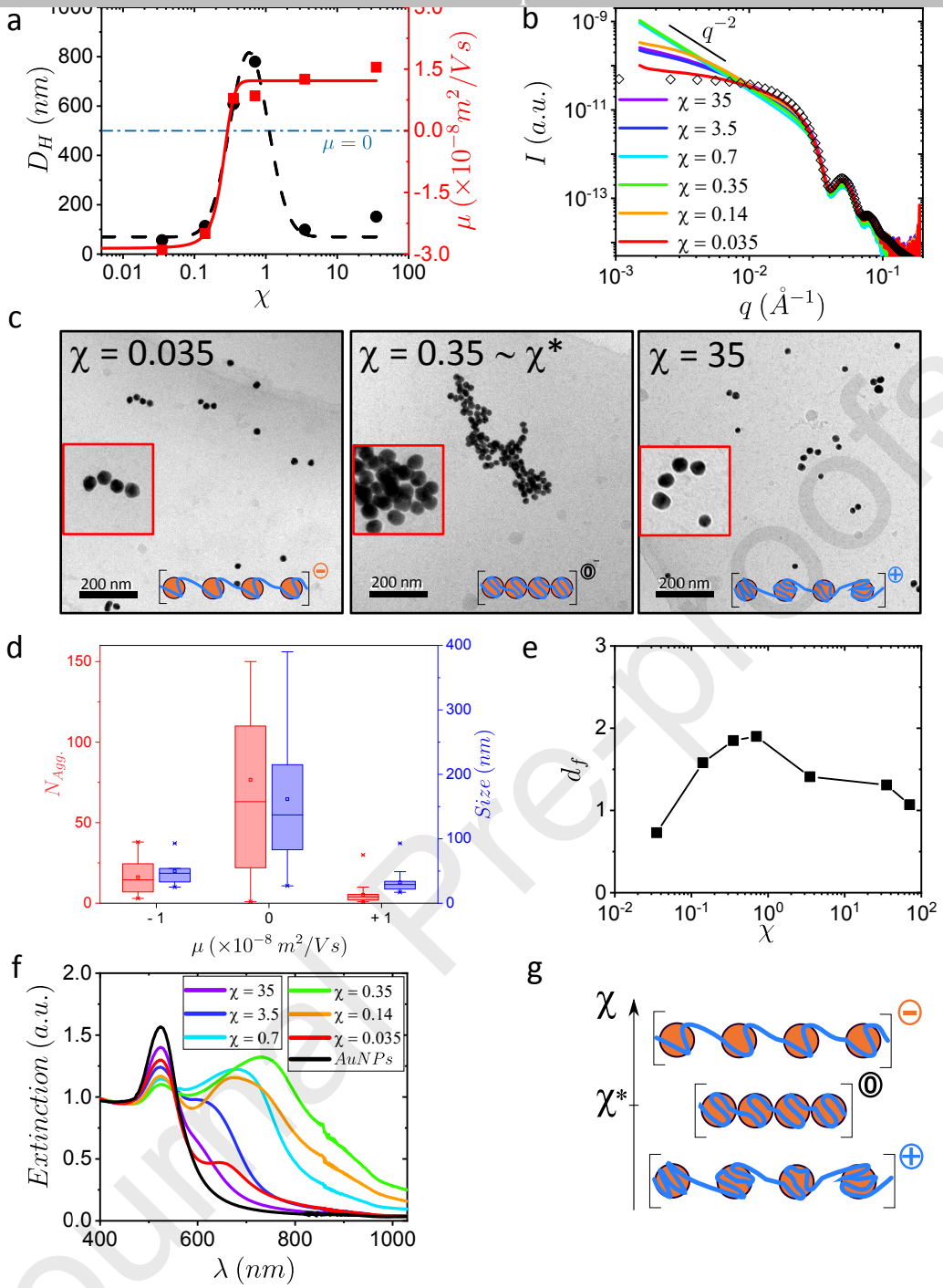

Figure 1. Characterizations of QC/AuNP assemblies ~2 min after formation. (a) Evolution of the electrophoretic mobility (μ, red square) and hydrodynamic diameter (D_H, black disc) versus the QC/AuNP molar ratio (χ). Lines are guides for the eye. (b) SAXS curves obtained for different χ. The black diamonds represent the form factor of spheres with a log. normal polydispersity (R = 11.5 nm; PDI = 0.1). (c) CryoTEM images obtained for three values of χ (i.e. 0.035, 0.35 and 35) corresponding to assemblies with negative, neutral and positive global charges. Enlargements are shown in inset.

Additional cryo-TEM images are shown in figure S3. (d) Evolution of averaged aggregation number ($N_{Agg.}$, red box) and size (blue box) determined by analysis of cryoTEM images for assemblies with different electrophoretic mobilities. (e) Mass fractal dimension (d_f) vs. χ. d_f has been determined by power-law fitting (i.e. $I \propto q^{-d_f}$) of the curves shown in figure 1b for $q < 0.025$ Å^{-1}. (f) UV-Vis. spectra obtained for different values of χ indicated on the plot. The curves were normalized to superimpose at

Interestingly, PEL chains were never detected because of their low concentration and low electronic contrast compared to AuNPs. In addition, the particles appears to be close together whatever the value of χ. However we underline the difficulty to measure the distance accurately due to the fragility of the ice with respect to the electron beam and the three-dimensional nature of the aggregates.

We performed UV−Vis.-NIR spectroscopy (Figure 1f) to shed light indirectly on the interparticle distance through the eventual detection of a collective absorption band arising from plasmonic coupling between adjacent particles. Overall, the complexation leads to a widening of the localized surface plasmon resonance (LSPR) band of individual AuNPs of around 525 nm when χ goes toward χ^* but staying within the range where finite size aggregates have been detected by DLS. Around χ^*, a second SPR band grows around 600 nm at the expense of the primary LSPR band. We analyze these results by considering that the presence of a secondary SPR band with a maximum at $\lambda \sim 730$ nm results from plasmon delocalization on the different particles of a given complex. Considering that the aggregates have almost the same internal structure whatever χ (Figures 1b , 1d, and S3), we believe that plasmon coupling is favored around χ^* due to a smaller interparticle distance and to a higher aggregation number. This is supported by numerical simulations showing the dependence of the absorption cross-section with these two parameters for fractal aggregates of gold particles.[32]

To clarify the global picture that emerges from this first part we used the comprehensive representation introduced by Nguyen and Shklovskii [10]. At low χ, the complexes are negatively charged nanoscale aggregates exhibiting a second SPR band of low amplitude with a maximum around 600 nm. In this case it is conceivable that the QCs wrap around the particles in such a way that they retain a locally negative charge after adsorption. The optical properties are in agreement with what can be expected for small aggregates as observed in cryoTEM.[32] On the other hand, high χ complexes, are nano-sized positively charged aggregates with low plasmon coupling. The local arrangement of the particles is comparable to the one observed previously, but the amount of QC/AuNP must be more important to allow a charge inversion of the particles. Around χ^*, the globally neutral complexes are denser, bigger and exhibit

collective plasmon band. In the following section we describe the method developped to stabilise these neutral aggregates by a second addition of PEL.

2.2 Stabilization of globally neutral complexes with long PEL chains.

UV−Vis.-NIR spectroscopy (Figure 2a and S6-7). In the absence of quenching agents and mixing the relative extinction at 400 nm decreases sharply after a characteristic time (t*) of about 40 min. At this time, large aggregates are formed and settle rapidly. Most of particles and QC chains are visibly concentrated at the bottom of the cuve after ~ 2 h. We underline that the temporal evolution of the relative extinction at 400 nm only allows an estimation of the evolution of the concentration of the particles in the medium because the growth of the aggregates leads to an increase of the scattering cross section, and thus also of the extinction, at this wavelength. This fast kinetic is not surprising if one considers that aggregates comprising ~ 83 particles of an element as dense as gold are already formed 2 min after mixing (Figure 1d-e). We then studied the effect of the subsequent addition of PEL (i.e. quenching agent) on this phase separation process by adding 1 mL of QC at different concentrations ($[QC]_{Quench}$) to a dispersion of neutral aggregates (V = 3 mL, [NP] = 6.8×10^{11} NPs.mL^{-1}) prepared a few seconds before. The main effect is an increase in the characteristic time (t*) with a relationship of the type $t^* \propto \sqrt{[QC]}$. At the same time the overall electrophoretic mobility of the samples becomes positive as soon as QC is added to the medium and increases in a monotonic manner with the addition of QC (Figure S8). We did not make measurements above 5 g/L because the samples become too viscous and difficult to handle (i.e. problem of homogeneity, bubble formation). However, if we refer to past studies[33] we can anticipate that at higher concentrations the phase separation process should be arrested without detectable sedimentation due to aggregate trapping in the 3D polymer network.

In the following, we will focus on the intermediate condition of quenching with $[QC]_{Quench}$ ≈ 0.5 g/L. In this concentration domain, the samples have a viscosity close to water and remain homogeneous for several hours (Video 1 in SI). Aggregates start to visibly settle down for times longer than one day (i.e. t* ~ 38 h). We emphasize that this evolution is different from a flocculation, a coacervation or a precipitation. Indeed, gentle hand mixing allows to reform an homogeneous sample with the same characteristics (UV-Vis, DLS, SAXS) as those obtained 2 min after mixing (Figure 2b-f). Individual gold particles also settle down on this time scale when their size is greater than 100 nm due to the density of gold.[34] Cryo-TEM observations, DLS and SAXS measurements (Figure 2c, 2e, 2f, S4-S5) show that quenched aggregates have

similar sizes and structures to the neutral complexes. These characteristics are clearly different from those of aggregates obtained by direct mixing with an excess of one of the partners (Figure 1) or by quenching with nanoparticles.[23,26] Thus, quenched aggregates contain particles in

not involved in the aggregates, is negligible.

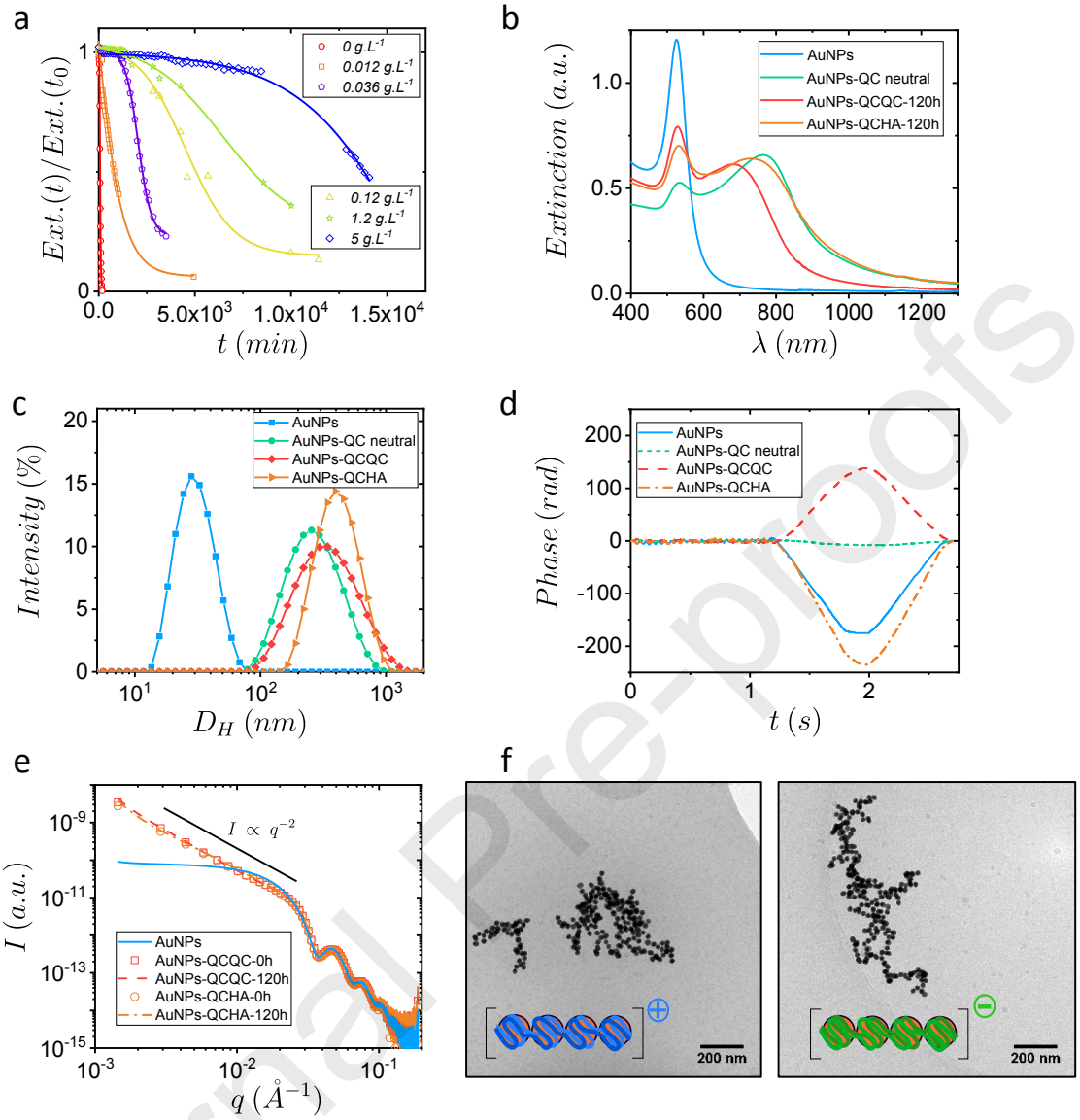

Figure 2. Characterizations of QC/AuNP electrostatic assemblies prepared at χ* before the addition of quenching PEL in a second step at different concentrations. (a) Temporal evolution of the relative extinction ($Ext.(t)/Ext.(t_{30s})$) determined at λ = 400 nm for different concentrations of quenching PEL as indicated in the figure. The concentrations shown in the figure correspond to the concentration of quenching PEL (and not of coupling PEL) after injection. In this case the quenching PEL is QC. (b) UV-Vis.-NIR spectra obtained for stabilized (AuNPs-QCQC and AuNPs-QCHA) samples 120 h after the injection of the stabilizing agent and for non-stabilized (AuNPs-QC neutral) samples 2 min after injection of the coupling agent. (c) Intensity weighted distribution of hydrodynamic diameters determined for stabilized and non-stabilized samples 2 min after mixing. (d) Temporal evolution of the phase during electrophoretic mobility measurements for electric field oscillating at 20 Hz (Time < 1.2 s) and then 0.2 Hz (Time > 1.2 s). The inset is an enlargement of the phase evolution during the first

second. (e) SAXS curves obtained for stabilized and non-stabilized samples 2 min and 120 h after coupling. (f) Typical cryoTEM images obtained after quenching with QC or HA. Complementary cryoTEM and UV-Vis caracterisations are shown in figures S4-S6-S7.

As can be expected for this type of aggregation at the ZCR, the quenched aggregates are

which the quench is performed with significant variations on the time scale of a second due to the high aggregation speed. Similarly, the UV-Vis-NIR spectra (Figure 2b) of suspensions of quenched aggregates show the same characteristics as those of neutral complexes (i.e., two SPR bands around 525 and 700 nm) but with significant variability in the amplitude of the bands depending on the time at which the aggregation is quenched. In Figure 2b, the variation in the amplitude of the band around 525 nm between the spectra of the neutral and quenched aggregates suggests that during the acquisition time of a UV-Vis-NIR spectrum, which is about 300 s, the neutral aggregates sediment more than the stabilized samples. We show in a video (SI) and a series of time-resolved UV-Vis measurements (Figure S7) with short acquisition time that it is indeed possible to freeze the optical properties of neutral aggregates using quaternized chitosan as quenching agent.

The aggregates obtained after quenching are positively charged (Figure 2d) with an electrophoretic mobility close to that of the aggregates prepared by direct coupling above χ^*.

In a second step, we studied the influence of a semi-flexible polyanion on the dynamic of AuNP/QC phase separation around χ^*. As a case study, we chose hyaluronic acid, noted HA, with Mw ≈ 177000 g/mol. We observed the same type of concentration-dependent behaviour as that observed with QC. Working at intermediate HA concentration, around 0.5 g/L, one could stabilise nanoscale aggregates (Figure 2c and S10) without structural (Figure 2e-f,S4) or optical (Figure 2e and S10) modification by giving them an overall negative charge (Figure 2d).

Although we cannot directly characterize the conformation of PEL chains on the surface of particles and aggregates without denaturing the system, the different results allow us to propose the following mechanism of stabilisation. At χ^*, the complexes are globally neutral but the particles constituting these complexes should be covered with an unsaturated layer of PEL so that the surface has both positive and negative charges. The presence of these domains allows the absorption, by electrostatic interaction, of additional PEL chains (i.e. cationic or anionic), until an homogeneous surface charge is established. Thus, as shown in figure 2 and S8, the progressive addition of PEL on neutral complexes leads to a progressive increase of the charge of the complexes (i.e. the electrophoretic mobility increases while the size does not change) until they are stabilised against aggregation by electrostatic repulsion.

In summary, we showed that the aggregation process occuring around χ^* could be arrested by the addition of long PEL chains and could lead to a dispersion of nanometric aggregates with a good colloidal stability. These aggregates have the size, structure and optical properties which can be cationic or anionic regardless of the coupling agent.

2.3 Colloidal stability of quenched aggregates.

To appreciate the robustness and applicative interest of the stabilisation process we studied the stability of quenched aggregates in different medias by UV-Vis. Spectroscopy (Figures S9-S11), DLS (Figures S9-S11) and SAXS (Figure 3). First, we have investigated the influence of dilution in milliQ water by means of SAXS measurements (Figure 3a). In contrast with DLS and UV-Vis spectroscopy, the high sensitivity of SAXS allowed us to detect the structural signature of the aggregates even after dilution by a factor 50. It appeared that the scattering pattern normalized by the particle concentration are superimposed over a period of 5 days if one gently shake the samples regularly to counterbalance the gravity driven sedimentation mentioned in section 2.2. This means that the average structure of the aggregates and their colloidal stability are not affected by dilution. Then, we investigated the influence of ionic strength. As shown in figure 3b, the dispersion of quenched aggregates in saline water have no effect on the scattering patterns over a period of 3 days for NaCl concentrations up to 0.15 M. We point out that, contrary to our expectations based on previous results,[18] the dispersion of the aggregates in a saline environment does not increase the fractal dimension of the aggregates. Similarly, the UV-Vis. spectra and hydrodynamic diameter distributions are not significantly affected by the concentration of NaCl, in the range studied, over a period of 3 days (Figure S9). We also showed that the colloidal stability of the aggregates stabilized by chitosan was maintained for 3 days at acidic pH (Figure S11). At this pH, the structure of the assemblies and their optical properties are not modified compared to the previous cases (Figure 3c and S11). In contrast with aggregates stabilized by chitosan, the stability of the aggregates stabilized by hyaluronic acid is less good than at pH 6.5 (Figure S11). This should be due to the protonation of carboxilic acid. All together, the fact of preserving colloidal and structural stability by dilution, lowering the pH and raising the ionic strength make practical applications credible. We emphasize that, although the influence of ionic strength and pH on the stabilized assemblies is small, it is probable that the structure of the assemblies can be modified by varying parameters such as temperature, pH and/or ionic strength at the coupling step (step 1). Indeed, these levers

are known to influence the diffusion and the electrostatic interactions controlling the assembly of QC and AuNPs.

To make a further step towards complexity we considered the dispersion of quenched

Remarkably, we observed different behaviours depending on the sign of the surface charge of the aggregates (Figure 3d). Indeed, the positively charged aggregates obtained with QC as quenching agent, present a lower colloidal stability than the negatively charged aggregates prepared with HA. The size and structure of the aggregates, seen by SAXS at t_0, being roughly the same, it suggests that the nature of the adsorbed proteins and/or their conformation at the aggregate's surface varies with the charge of the polymer covering the aggregates. Such influence of surface charge on the nature and dynamics of protein corona formation has been demonstrated in various studies using cationic or anionic gold particles dispersed in different types of culture media.[35,36] This result is interesting in the perspective of applications in biological environments.

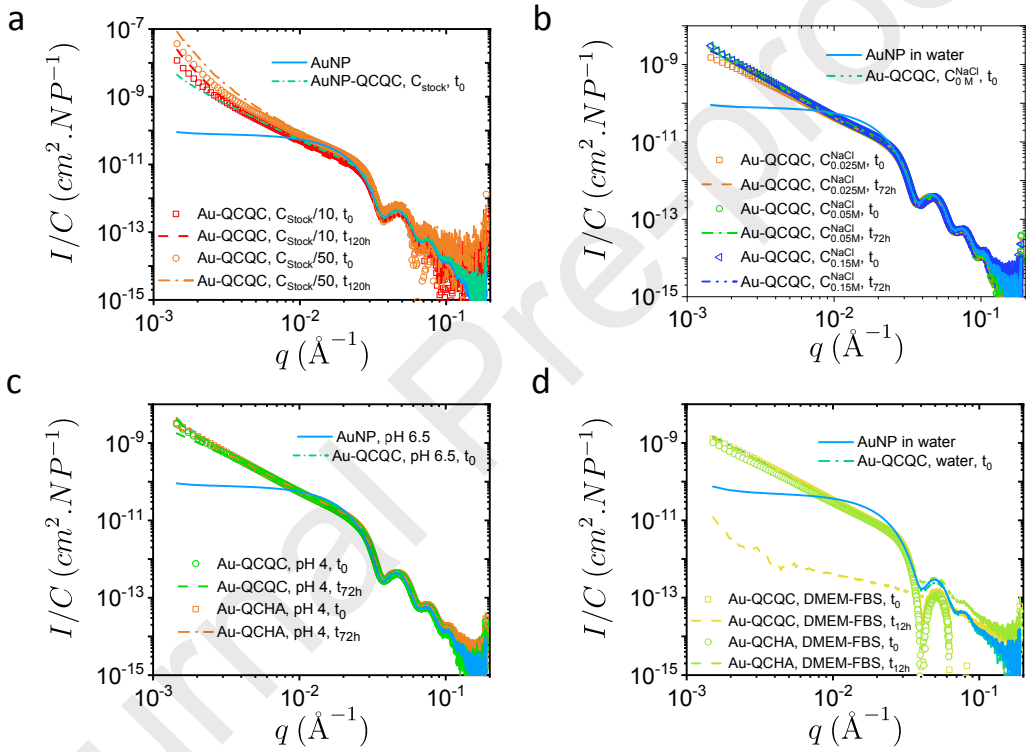

Figure 3. SAXS characterizations of quenched aggregates (Au-QCQC or Au-QCHA) at different times after dispersion in different media. (a) Dilution in milliQ water by a factor 1 (i.e. no dilution), 10 and 50. (b) Dilution by a factor two in NaCl aqueous solutions with NaCl concentration (C^{NaCl}) ranging from 0 to 0.15 M. (c) Dilution by a factor two in NaCl aqueous solutions with NaCl concentration (C^{NaCl}) ranging from 0 to 0.15 M. (d) Dilution by a factor two in acid (pH 3, H_2O-HCl) or basic media (pH 12, H_2O-NaOH). (d) Dilution by a factor two in DMEM-FBS (10 %) media without phenol red. After 12 h all samples were gently shaken 5 min before measurement to counterbalance the gravity driven sedimentation mentioned in section 2.2. Data obtained by DLS and UV-Vis. spectroscopy for the same

types of samples, except for diluted samples and those dispersed in 10% DMEM-FBS medium, are presented in Figures S9-S11.

3. Conclusion

In this article we show that electrostatic complexes of polyelectrolytes (PEL) and nanoparticles formed at the net zero charge ratio could be stabilized by the subsequent addition of long polyelectrolyte chains. The colloidal stabilisation is demonstrated by using polylectrolyte chains of biological origin and gold nanoparticles in saline environments, at different pH, as well as in cell culture media over periods of several days. Contrarily to protocols developed in the past to stabilize globally neutral complexes by adding nanoparticles, PEL-stabilized complexes are found to retain their initial characteristics/properties (i.e. shape, size, internal structure and optical properties) after stabilization. Hence, the plasmonic coupling allows to maximize the optical absorption around the 800 nm wavelength at which the lasers used for thermoplasmonic and surface enhanced Raman scattering analysis operate. Furthermore, the charge of the stabilizing chains (i.e. polyanions or polycations) determines the global charge of the stabilized complexes whatever the charge of the polylectrolyte used to form the globally neutral complex. Overall, our results provide new opportunities to master "flocculation assembly" by allowing the formation of finite size assemblies in which the inter-particle distance is minimal and the surface chemistry is adjustable. We anticipate that our approach based on electrostatic interactions between common compounds can be transposed to other systems (i.e., nanoparticles and PEL) with similar characteristics to the system studied in this paper. However, it is likely that structural parameters such as particle size will influence the stabilization process described in this paper because of the dependence of the interaction forces on such parameter. From an applicative point of view, we believe that our approach based on widely available polyelectrolytes of biological origin could facilitate the development of plasmonic applications that are currently limited by the difficulty of obtaining, in a quick and easy way, plasmonic active substrates with reproducible structures in different environments.

Experimental Section

Materials. Gold (III) chloride trihydrate ($HAuCl_4.3H_2O$, > 99.99 %), trisodium citrate dihydrate ($Na_3C_6H_5O_7.2H_2O$, ≥ 99 %), acetone (C_3H_6O, 99.5 %), chitosan ($C_8H_{13}NO_5$, degree of N-deacetylation ~ 75 %, M_w ~ 310-375 kg/mol according to the supplier and ~ 380 kg/mol after SEC measurement) were purchased from Sigma-Aldrich. Glycidyltrimethylammonium chloride, noted GTMAC ($C_6H_{14}ClNO$, 80 wt% in water) was purchased from Tokyo Chemical Industry. Sodium hyaluronate from bacterial fermentation ($C_{14}H_{20}NO_{11}Na$, M_w ~ 177 kg/mol according to SEC measurement) was provided under the name BASHYAL by Soliance (Givaudan SA). All solutions were prepared with milliQ water (R = 18.2 MΩ).

Gold Nanoparticles (AuNPs) synthesis. Citrate stabilized gold nanoparticles were first synthesized by seeded growth protocol proposed by N.G. Bastús *et al.* **developped**.**[37]** All the content of a gold salt powder was used at the first opening to prepare, using a glass spatula, a stock at 10 g/L that was stored for period not exceeding 3 months in dark. All glassware and teflon-coated magnetic bars were washed thoroughly with freshly prepared aqua regia and rinsed with milliQ water after each synthesis. Briefly, 97 mg of citrates (0.33 mmol) were put in 150 mL of water (2.2 mM solution) and refluxed for 15min, before adding 1 mL of a 10 g/L solution of $HAuCl_4.3H_2O$.**[38]** The solution was kept on reflux for 10 min, then the heating was slowly cooled down to 90 °C. The seeds had their size increased by repeating several growing cycles as followed: 55 mL of the solution were withdrawn, followed by the addition of 53 mL of water and 1 mL of a 60 mM citrates solution. As soon as the temperature reached 90 °C again, 1 mL of $HAuCl_4$ were added and the solution was stirred for 30 min. Then, 1 mL of $HAuCl_4$ were added and the solution was stirred again for 30 min. These growing cycles were repeated up to the desired size of AuNPs. Typically, 4 cycles were required to obtain particles with an diameter D_H ~ 22 nm. Between the seeds and the fourth cycle, theoretical gold nanoparticles concentration varies from 3.0×10^{12} NPs/mL to 4.8×10^{11} NPs/mL. The characterizations of the nanoparticles used in this study are presented in figure S1 of the supporting information (SI).

Chitosan quaternization. Citrate particles are stable in water and negatively charged at pH > 4 whereas chitosan is soluble in water and fully positively charged at pH < 4.5.

There is therefore a narrow pH window for coupling citrate particles and chitosan. However, to avoid any problems related to pH adjustment, we decided to quaternise the chitosan so that it is soluble in water and positively charged regardless of pH. This also

chitosan (QC) was synthetized in aqueous medium by ring opening between the chitosan's primary amine and the epoxy cycle of glycidyltrimethylammonium chloride (GTMAC). The protocol was adapted from literature.[39,40]

In a 250 mL two necked round bottom flask, 6 g of chitosan powder (see Materials section) was dispersed in 60 mL of milliQ water at 85 °C at reflux with a heating mantle during 2 hours leading to a suspension of partially solubilized chitosan (pH ≈ 6.5). 6.20 mL of glycidyltrimethylammonium chloride, noted GTMAC, was then added three times every two hours. The viscous yellow mixture was kept under magnetic stirring at 800 rpm during ~ 10 h. The polymer was 'precipitated' adding an excess of acetone and washed with acetone several times. After drying in oven at 60°C during two days one typically recovers 16 g of the polymer in the form of a yellow vitreous solid. It was then purified by dispersion in milliQ water at pH 6.5 and dialysed (cutoff ~ 14 kda) against milliQ water during four days to eliminate unreacted GTMAC. The water was changed every three hours. One finally recovers quaternized chitosan (QC) after freeze drying (~ 24 h).

Substitution degree (SD) was determined by conductimetric titration of chloride (23.4 mg of quaternized chitosan) with silver nitrate (0.01 M) and expressed as a percentage of the initial number of deacetylated groups. As shown in Figure S2, SD could be varied between 74 % and 104 % by modifiying the GTMAC/chitosan molar ratio between 2:1 and 4.5:1 in qualitative agreement with previous studies. We point out that SD could exceed 100% due to the occurance of different reactions such as (i) a second reaction with the amine or (ii) a reaction between GTMAC and hydroxy groups.

Name	**Acronym**	M_w^{PEL} **g/mole**	$M_w^{monomer}$ **g/mole**	L_c **nm**	**σ e/nm**
Chitosan	C	**357000**	**166**	**1075**	**1.5**
Sodium Hyaluronate	HA	**177000**	**401**	**441**	**1**

Table 1. Main characteristics of the polyelectrolytes (PEL) used in this study with their acronym: mass averaged molecular mass of the PEL (M_w^{PEL}) determined by size exclusion chromatography, molecular mass of the monomer ($M_w^{Monomer}$) contour length (L_c), structural linear charge density (σ). L_c and σ were calculated assuming a monomer size of 5 Å and 10 Å for C and HA respectively. The chitosan described in the table is the one on which the quaternization was performed.

All the experiments presented in the article were carried out with the same batch of QC

electrophoretic mobility, μ = + 4.7 μmcm/Vs. The characterizations of the polymers are presented together with polymer-specific characterization methods in the SI.

Particles self-assembly. AuNPs and PELs solutions were prepared separately in milliQ water and mixed together at 50 : 50 volume ratio. Thus the final concentration of gold particles is typically of the order of 2.4×10^{11} NPs/mL. This concentration is comparable to the concentration of particles used in the field of thermoplasmonics such as AuroShell™ particles marketed by the company Nanospectra Biosciences which are sold at a concentration of ~ 2.8×10^{11} particles/mL. Gold nanoparticles concentration remains constant for each mixture, the concentration in polymer varies in order to obtain severals molar ratio $\chi = {n_{polymer}}/{n_{AuNPs}}$ ($35*10^{-4} < \chi < 35$). Mixtures were mixed 3s with a vortex to ensure homogenization and then characterized in UV-Vis, DLS and electrophoretic mobility.

Methods.

Dynamic light scattering (DLS) experiments were carried out with a NanoZS apparatus (Malvern Instrument) operating at λ = 632.8 nm and P ≤ 4 mW. The fluctuations of the scattered intensity with time, noted I(q,t), was measured at fixed angle Θ = 173 ° or, equivalently, at a given scattering wave vector whose norm is $q = (4\pi n/\lambda)\sin(\theta/2)$ with n the solvant refractive index. These fluctuations reflect the brownian motion of the scattering objects. I(q,t) is first transformed into the normalized time auto-correlation function of the scattered intensity: $g^{(2)}$ (q,t). For a diffusive process, $g^{(2)}(q,t)\sim e^{-2qDt}$ with D the mutual diffusion coefficient. The hydrodynamic radius, R_H, of the brownian objects is determined with the Stokes–Einstein relation. The size distribution was derived from the inverse Laplace transform of the correlation function approximated with the CONTIN algorithm.

Laser Doppler velocimetry. Electrophoretic mobility (μ) was measured with a NanoZS apparatus (Malvern Instrument). This set-up operates with an electrical field of 25 $V.cm^{-1}$ oscillating successively at 20 Hz and 0.7 Hz to reduce the electroosmosis effect due to the surface charge of the capillary cell. The particle' velocity was measured by LASER Doppler velocimetry.

Ultraviolet visible spectroscopy (UV-vis) was performed on Cary 50 Scan UV-Visible spectrophotometer (Varian). The 5 mm thickness Hellma cell (quartz) were filled in by the diluted AuNPs solutions. The extinction values were recorded after baseline correction. `

performed on a Perkin Elmer Lambda 1050 spectrophotometer. 5 mm thickness Hellma cell (quartz) were filled in by the diluted AuNPs, QC and PEL. The diffuse transmission was measured by collecting the light exiting the sample using an integrating sphere (Perkin Elmer Accessory). Spectra were corrected from the quartz cell filled in with water.

Cryogenic transmission electron microscopy (cryo-TEM) images were taken on an Ultrascan 1000, 2k x 2 k CCD camera (Gatan, USA), using a LaB_6 JEOL JEM 2100 (JEOL, Japan) cryo-microscope operating at 200 kV with a JEOL low dose system (Minimum Dose System, MDS) to protect the thin ice film from any irradiation before imaging and to reduce the irradiation during the image capture. The images were recorded at 93 K.

Small angle X-ray scattering (SAXS) experiments were performed on SWING beamline (SOLEIL synchrotron, Saint-Aubin, France) with a photon energy of 12 keV and a sample-to-detector (Eiger 4M) distance of 6 m leading to the following q-ranges: $0.0016 \leq q\ (Å^{-1}) \leq 0.23$. We recall that the norm of the scattering wave vector is $q = (4\pi/\lambda)\sin(\theta/2)$, where θ is the scattering angle and λ = 1.033 Å is the wavelength. Samples were inserted into cylindrical quartz capillaries of 1.5 mm diameter that were sealed and left vertical in the field of gravity. Typically, 10 successive frames of 0.5 s each were recorded and compared to check the absence of beam damage. The scattering patterns were always isotropic. Each frame was first angularly averaged over all frames and the pure solvent spectrum was subtracted.

In general, our SAXS patterns are characterized by a power law decay of $I(q)$ for $q < 0.025$ $Å^{-1}$. At first order, we considered that this evolution reflects the mass-fractal scaling of the aggregates with q.[41,42] Therefore, the power law exponent obtained by fitting the curves with a power law function on one decade of q yields the mass fractal dimension (i.e. $I \propto q^{-d_f}$) as defined in the introduction. We underline that this simple analysis leads us to underestimate the fractal dimension of the aggregates obtained for $\chi < 0.14$ due to the presence of individual particles in equilibrium whose contribution to the scattered signal is not taken into account. We consider that this approximation is not critical in this study dedicated to the stabilization of aggregates obtained at $\chi \approx \chi^*$ without the coexistence of individual particles.

ANR (Agence Nationale de la Recherche) and CGI (Commissariat à l'Investissement d'Avenir) are gratefully acknowledged for their financial support of this work through Labex SEAM (Science and Engineering for Advanced Materials and devices). F.C. and F.V. thank the ANR Coligomere-18-CE0006 for funding. We are indebted to N. Sanson (Soft Matter Sciences and Engineering, ESPCI, PSL University, Sorbonne Université, CNRS) for his assistance during preliminary TOC measurements. We acknowledge the technopolym platform (Université de Toulouse III-Paul Sabatier) for SEC and TOC measurements. We also acknowledge synchrotron SOLEIL (SWING beam line, Saint-Aubin, France) for the SAXS beam time allocation.

References.

[1] H.G.B. Jong, H.R. Kruyt, Koazervation: Entmischung in kolloiden Systemen, Kolloid-Zeitschrift. 50 (1930) 39–48. https://doi.org/10.1007/BF01422833.
[2] T.L. Pugh, W. Heller, Coagulation and stabilization of colloidal solutions with polyelectrolytes, Journal of Polymer Science. 47 (1960) 219–227. https://doi.org/10.1002/pol.1960.1204714919.
[3] D.H. Napper, Polymeric stabilization of colloidal dispersions, Academic Press, London, 1983.
[4] G. Schneider, G. Decher, Functional Core/Shell Nanoparticles via Layer-by-Layer Assembly. Investigation of the Experimental Parameters for Controlling Particle Aggregation and for Enhancing Dispersion Stability, Langmuir. 24 (2008) 1778–1789. https://doi.org/10.1021/la7021837.
[5] O. Spalla, B. Cabane, Growth of colloidal aggregates through polymer bridging, Colloid & Polymer Science. 271 (1993) 357–371. https://doi.org/10.1007/BF00657417.
[6] O. Spalla, Nanoparticle interactions with polymers and polyelectrolytes, Current Opinion in Colloid & Interface Science. 7 (2002) 179–185. https://doi.org/10.1016/S1359-0294(02)00045-6.
[7] J.-P. Chapel, J.-F. Berret, Versatile electrostatic assembly of nanoparticles and polyelectrolytes: Coating, clustering and layer-by-layer processes, Current Opinion in Colloid & Interface Science. 17 (2012) 97–105. https://doi.org/10.1016/j.cocis.2011.08.009.
[8] R.R. Netz, J.-F. Joanny, Complexation between a Semiflexible Polyelectrolyte and an Oppositely Charged Sphere, Macromolecules. 32 (1999) 9026–9040. https://doi.org/10.1021/ma990264+.
[9] S. Ulrich, A. Laguecir, S. Stoll, Complexation of a Weak Polyelectrolyte with a Charged Nanoparticle. Solution Properties and Polyelectrolyte Stiffness Influences, Macromolecules. 38 (2005) 8939–8949. https://doi.org/10.1021/ma051142m.
[10] T.T. Nguyen, B.I. Shklovskii, Complexation of DNA with positive spheres: Phase diagram of charge inversion and reentrant condensation, The Journal of Chemical Physics. 115 (2001) 7298–7308. https://doi.org/10.1063/1.1402988.
[11] K. Keren, Y. Soen, G.B. Yoseph, R. Gilad, E. Braun, U. Sivan, Y. Talmon, Microscopics of Complexation between Long DNA Molecules and Positively Charged Colloids, Physical Review Letters. 89 (2002). https://doi.org/10.1103/PhysRevLett.89.088103.

[12] A.A. Zinchenko, K. Yoshikawa, D. Baigl, Compaction of Single-Chain DNA by Histone-Inspired Nanoparticles, Physical Review Letters. 95 (2005). https://doi.org/10.1103/PhysRevLett.95.228101.
[13] L. Shi, F. Carn, F. Boue, G. Mosser, E. Buhler, Nanorods of Well-Defined Length and Monodisperse Cross-Section Obtained from Electrostatic Complexation of Nanoparticles with a

https://doi.org/10.1021/mz300200y.
[14] L. Shi, F. Carn, F. Boue, G. Mosser, E. Buhler, Control over the electrostatic self-assembly of nanoparticle semiflexible biopolyelectrolyte complexes, Soft Matter. 9 (2013) 5004–5015. https://doi.org/10.1039/c3sm27138b.
[15] L. Shi, E. Buhler, F. Boué, F. Carn, Shape-Tailored Colloidal Molecules Obtained by Self-Assembly of Model Gold Nanoparticles with Flexible Polyelectrolyte, Langmuir. 31 (2015) 5731–5737. https://doi.org/10.1021/acs.langmuir.5b00854.
[16] M.. Lin, R. Klein, H.. Lindsay, D.. Weitz, R.. Ball, P. Meakin, The structure of fractal colloidal aggregates of finite extent, Journal of Colloid and Interface Science. 137 (1990) 263–280. https://doi.org/10.1016/0021-9797(90)90061-R.
[17] R. Jullien, R. Botet, Aggregation and fractal aggregates, World Scientific Publishing, Singapore, 1987.
[18] L. Shi, F. Carn, F. Boue, E. Buhler, Role of the ratio of biopolyelectrolyte persistence length to nanoparticle size in the structural tuning of electrostatic complexes, Physical Review E. 94 (2016) 032504. https://doi.org/10.1103/PhysRevE.94.032504.
[19] M. Jonsson, P. Linse, Polyelectrolyte–macroion complexation. II. Effect of chain flexibility, The Journal of Chemical Physics. 115 (2001) 10975–10985. https://doi.org/10.1063/1.1417508.
[20] L. Shi, F. Carn, A. Goukassov, E. Buhler, F. Boué, Self-Induced Crystallization in Charged Gold Nanoparticle-Semiflexible Biopolyelectrolyte Complexes, Langmuir. 36 (2020) 7925–7932. https://doi.org/10.1021/acs.langmuir.0c01064.
[21] L. Novotny, B. Hecht, Principles of nano-optics, Cambridge University Press, Cambridge, 2012.
[22] G. Baffou, F. Cichos, R. Quidant, Applications and challenges of thermoplasmonics, Nature Materials. 19 (2020) 946–958. https://doi.org/10.1038/s41563-020-0740-6.
[23] V.S. Murthy, J.N. Cha, G.D. Stucky, M.S. Wong, Charge-Driven Flocculation of Poly(L -lysine)Gold Nanoparticle Assemblies Leading to Hollow Microspheres, Journal of the American Chemical Society. 126 (2004) 5292–5299. https://doi.org/10.1021/ja038953v.
[24] V.S. Murthy, S.B. Kadali, M.S. Wong, Polyamine-Guided Synthesis of Anisotropic, Multicompartment Microparticles, ACS Applied Materials & Interfaces. 1 (2009) 590–596. https://doi.org/10.1021/am8001499.
[25] S.E. Plush, M. Woods, Y.-F. Zhou, S.B. Kadali, M.S. Wong, A.D. Sherry, Nanoassembled Capsules as Delivery Vehicles for Large Payloads of High Relaxivity Gd $^{3+}$ Agents, Journal of the American Chemical Society. 131 (2009) 15918–15923. https://doi.org/10.1021/ja906981w.
[26] R.K. Rana, V.S. Murthy, J. Yu, M.S. Wong, Nanoparticle Self-Assembly of Hierarchically Ordered Microcapsule Structures, Advanced Materials. 17 (2005) 1145–1150. https://doi.org/10.1002/adma.200401612.
[27] J. Yu, D. Javier, M.A. Yaseen, N. Nitin, R. Richards-Kortum, B. Anvari, M.S. Wong, Self-Assembly Synthesis, Tumor Cell Targeting, and Photothermal Capabilities of Antibody-Coated Indocyanine Green Nanocapsules, Journal of the American Chemical Society. 132 (2010) 1929–1938. https://doi.org/10.1021/ja908139y.
[28] G.F. Schneider, G. Decher, From “Nano-bags” to “Micro-pouches”. Understanding and Tweaking Flocculation-based Processes for the Preparation of New Nanoparticle-Composites, Nano Letters. 8 (2008) 3598–3604. https://doi.org/10.1021/nl801511w.
[29] A. Balfourier, V. Mulens-Arias, F. Gazeau, F. Carn, Rational Design of Fractal Gold Nanosphere Assemblies with Optimized Photothermal Conversion Using a Quantitative Structure Property Relationship (QSPR) Approach, The Journal of Physical Chemistry C. 124 (2020) 8938–8948. https://doi.org/10.1021/acs.jpcc.0c00384.
[30] S. Franco-Ulloa, G. Tatulli, S.L. Bore, M. Moglianetti, P.P. Pompa, M. Cascella, M. De Vivo, Dispersion state phase diagram of citrate-coated metallic nanoparticles in saline solutions, Nat Commun. 11 (2020) 5422. https://doi.org/10.1038/s41467-020-19164-3.

[31] L. Belloni, Electrostatic interactions in colloidal solutions: Comparison between primitive and one-component models, The Journal of Chemical Physics. 85 (1986) 519–526. https://doi.org/10.1063/1.451629.
[32] B. Khlebtsov, V. Zharov, A. Melnikov, V. Tuchin, N. Khlebtsov, Optical amplification of photothermal therapy with gold nanoparticles and nanoclusters, Nanotechnology. 17 (2006)

[33] I. Morfin, E. Buhler, F. Cousin, I. Grillo, F. Boué, Rodlike Complexes of a Polyelectrolyte (Hyaluronan) and a Protein (Lysozyme) Observed by SANS, Biomacromolecules. 12 (2011) 859–870. https://doi.org/10.1021/bm100861g.
[34] J. Midelet, A.H. El-Sagheer, T. Brown, A.G. Kanaras, M.H.V. Werts, The Sedimentation of Colloidal Nanoparticles in Solution and Its Study Using Quantitative Digital Photography, Part. Part. Syst. Charact. 34 (2017) 1700095. https://doi.org/10.1002/ppsc.201700095.
[35] E. Casals, T. Pfaller, A. Duschl, G.J. Oostingh, V. Puntes, Time Evolution of the Nanoparticle Protein Corona, ACS Nano. 4 (2010) 3623–3632. https://doi.org/10.1021/nn901372t.
[36] T.L. Moore, L. Rodriguez-Lorenzo, V. Hirsch, S. Balog, D. Urban, C. Jud, B. Rothen-Rutishauser, M. Lattuada, A. Petri-Fink, Nanoparticle colloidal stability in cell culture media and impact on cellular interactions, Chemical Society Reviews. 44 (2015) 6287–6305. https://doi.org/10.1039/C4CS00487F.
[37] N.G. Bastús, J. Comenge, V. Puntes, Kinetically Controlled Seeded Growth Synthesis of Citrate-Stabilized Gold Nanoparticles of up to 200 nm: Size Focusing versus Ostwald Ripening, Langmuir. 27 (2011) 11098–11105. https://doi.org/10.1021/la201938u.
[38] L. Shi, E. Buhler, F. Boue, F. Carn, How does the size of gold nanoparticles depend on citrate to gold ratio in Turkevich synthesis? Final answer to a debated question, Journal of Colloid and Interface Science. 492 (2017) 191–198. https://doi.org/10.1016/j.jcis.2016.10.065.
[39] E. Loubaki, M. Ourevitch, S. Sicsic, Chemical modification of chitosan by glycidyl trimethylammonium chloride. characterization of modified chitosan by 13C- and 1H-NMR spectroscopy, European Polymer Journal. 27 (1991) 311–317. https://doi.org/10.1016/0014-3057(91)90111-Z.
[40] S.-H. Lim, S.M. Hudson, Synthesis and antimicrobial activity of a water-soluble chitosan derivative with a fiber-reactive group, Carbohydrate Research. 339 (2004) 313–319. https://doi.org/10.1016/j.carres.2003.10.024.
[41] G. Beaucage, Small-Angle Scattering from Polymeric Mass Fractals of Arbitrary Mass-Fractal Dimension, J Appl Crystallogr. 29 (1996) 134–146. https://doi.org/10.1107/S0021889895011605.
[42] T. Li, A.J. Senesi, B. Lee, Small Angle X-ray Scattering for Nanoparticle Research, Chemical Reviews. 116 (2016) 11128–11180. https://doi.org/10.1021/acs.chemrev.5b00690.

Credit author

Florent Voisin: Investigation, Methodology, Writing, Project administration. **Gérald Lelong**: Investigation, Methodology, Reviewing. **Thomas Bizien**: Investigation, Methodology, Reviewing. **Jean-Marie Guigner**: Investigation, Methodology, Reviewing. ***Jean-Maurice Mallet****:* Supervision, Methodology, Reviewing. **Florent Carn:** Conceptualization, Methodology, Supervision, Writing, Funding acquisition.

Graphical abstract

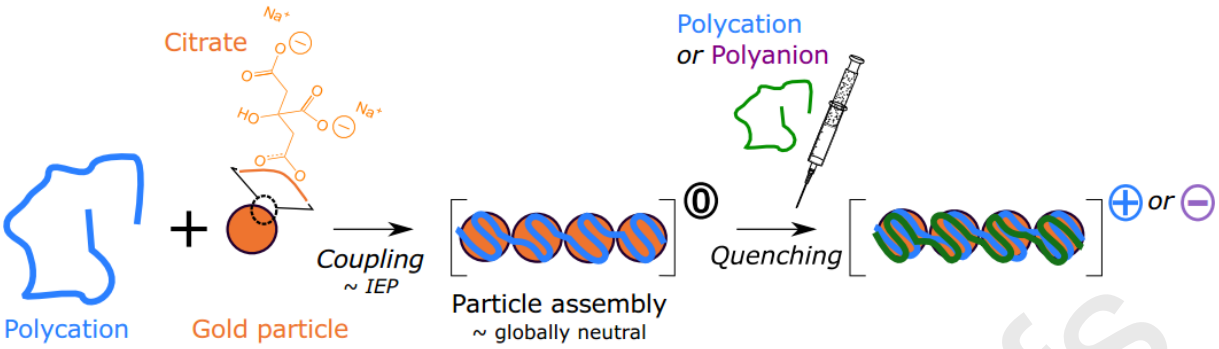

Declaration of interests

☐ The authors declare that they have no known competing financial interests or personal relationships that could have appeared to influence the work reported in this paper.

☒ The authors declare the following financial interests/personal relationships which may be considered as potential competing interests:

Florent CARN reports financial support was provided by French National Research Agency.